Journal of Materials Chemistry B

Accepted Manuscript

 Journal of Materials Chemistry B

Journal of
Materials Chemistry B

Cite this: DOI: 10.1039/c0xx00000x

www.rsc.org/xxxxxx

PAPER

Facile synthesis of folic acid-functionalized iron oxide nanoparticles with ultrahigh relaxivity for targeted tumor MR imaging†

Jingchao Li,[a1] Yong Hu,[a1] Jia Yang,[b1] Wenjie Sun,[a] Hongdong Cai,[c] Ping Wei,[a] Yaping Sun,[d]* Guixiang Zhang,[b] Xiangyang Shi,[a, c]* Mingwu Shen[a]*

Received (in XXX, XXX) Xth XXXXXXXXX 20XX, Accepted Xth XXXXXXXXX 20XX
DOI: 10.1039/b000000x

We present the polyethyleneimine (PEI)-assisted synthesis of folic acid (FA)-functionalized iron oxide (Fe_3O_4) nanoparticles (NPs) with ultrahigh relaxivity for *in vivo* targeted tumor magnetic resonance (MR) imaging. In this work, water-dispersible and stable Fe_3O_4 NPs were synthesized in the presence of PEI *via* a facile mild reduction approach. The surface PEI coating afforded the formed Fe_3O_4 NPs with the ability to be functionalized with polyethylene glycol (PEG)-linked FA and fluorescein isothiocyanate (FI). A further acetylation step to neutralize the remaining PEI surface amines gave rise to the formation of multifunctional FA-functionalized Fe_3O_4 NPs, which were subsequently characterized *via* different methods. We show that the developed FA-functionalized Fe_3O_4 NPs have a good water-dispersibility, good colloidal stability, ultrahigh r_2 relaxivity (475.92 $mM^{-1}s^{-1}$), and good hemocompatibility and cytocompatibility in the studied concentration range. The targeting specificity of the FA-modified Fe_3O_4 NPs to FA receptors (FAR)-overexpressing HeLa cells (a human cervical carcinoma cell line) was subsequently validated by flow cytometry and confocal microscopy. Significantly, the developed FA-modified Fe_3O_4 NPs can be used as a nanoprobe for targeted MR imaging of HeLa cells *in vitro* and the xenografted tumor model *in vivo via* an active FA-mediated targeting strategy. The developed multifunctional FA-modified Fe_3O_4 NPs with an ultrahigh r_2 relaxivity may be used as an efficient nanoprobe for targeted MR imaging of various kinds of FAR-overexpressing tumors.

Introduction

Various nanomaterials have been constructed for the diagnosis and treatment of cancer with the progress of nanotechnology.[1-5] Especially, magnetic iron oxide (Fe_3O_4) nanoparticles (NPs) have been extensively applied for magnetic resonance (MR) imaging of different biological systems owing to their excellent biocompatibility and magnetic property.[6-8] Due to the size-dependent magnetic properties,[9] superparamagnetic Fe_3O_4 NPs with a size below 20 nm have been utilized as negative contrast agents for T_2-weighted MR imaging,[10-12] whereas ultrasmall superparamagnetic Fe_3O_4 NPs (diameter < 5 nm) have recently been applied for positive T_1-weighted MR imaging.[13-15] In either case, for MR imaging with high sensitivity, it is essential to synthesize Fe_3O_4 NPs possessing high relaxivity. Various methods have been utilized to synthesize Fe_3O_4 NPs for T_1- or T_2-weighted MR imaging applications such as controlled co-precipitation, thermal decomposition, and hydrothermal synthesis.[16-19] Unfortunately, none of them is able to produce single Fe_3O_4 NPs with ultrahigh relaxivity (e.g., r_2 relaxivity ≥ 200 $mM^{-1}s^{-1}$), quite limiting their practical applications in highly sensitive MR imaging.

Recently, a new mild reduction method was used to synthesize Fe_3O_4 NPs that can be encapsulated by polymer *via* a photochemical polymerization method.[20] Due to the fact that the used method to synthesize Fe_3O_4 NPs is quite different from the above mentioned approaches, we tried to functionalize such type of Fe_3O_4 NPs for biomedical imaging applications. The surface modification was aiming to overcome the colloidal instability of Fe_3O_4 NPs induced by the magnetic dipole interaction and their inherently large surface energy.[21-23]

Previously we have succeeded in the synthesis of 3-aminopropyltriethoxysilane (APTS)- and polyethyleneimine (PEI)-coated Fe_3O_4 NPs *via* a one-pot hydrothermal approach.[24, 25] The dense primary amine groups on the surface of Fe_3O_4 NPs rendered by the APTS or PEI coating not only endow the NPs with colloidal stability, but also mediates convenient modification and functionalization of the particle surfaces for various biomedical applications. For instance, the surface modification of polyethylene glycol (PEG) onto the PEI-coated Fe_3O_4 NPs afforded the particles with improved cytocompatibility and reduced macrophage uptake.[25-27] In addition, the PEI-coated Fe_3O_4 NPs were able to be covalently linked with PEGylated folic acid (FA)[28] or hyaluronic acid (HA)[29] for targeted MR imaging of tumors overexpressing FA receptors (FAR) or CD44 receptors, respectively. These earlier successes stimulate us to deduce that PEI-coated Fe_3O_4 NPs might also be synthesized *via* a mild reduction method and be functionalized with PEGylated FA for targeted MR imaging of FAR-overexpressing tumors.

In this current work, we report a convenient approach to forming colloidally stable FA-functionalized Fe_3O_4 NPs for targeted tumor MR imaging. Water-dispersible PEI-coated Fe_3O_4 NPs were first prepared, and then sequentially modified with PEGylated FA and fluorescein isothiocyanate (FI) *via* PEI-mediated conjugation chemistry. The remaining PEI surface amines were subjected to acetylation to form the multifunctional FA-functionalized Fe_3O_4 NPs (Scheme 1), which were subsequently characterized using different methods. Surprisingly, the formed FA-functionalized Fe_3O_4 NPs displayed an ultrahigh r_2 relaxivity (475.92 $mM^{-1}s^{-1}$). Quantitative cell viability assay, observation of cell morphology, and hemolysis assay were employed to evaluate the cytotoxicity and hemocompatibility of the particles, respectively. The targeting specificity of the multifunctional particles to FAR-overexpressing HeLa cells (a human cervical carcinoma cell line) *in vitro* were evaluated by flow cytometry and confocal microscopy. Furthermore, the potential to use the developed FA-functionalized Fe_3O_4 NPs as a nanoprobe for MR imaging of HeLa cells *in vitro* and the xenografted tumor model *in vivo* was also explored. To the best of our knowledge, this is the first study associated to the mild reduction synthesis of Fe_3O_4 NPs with an ultrahigh r_2 relaxivity for targeted MR imaging of tumors.

Experimental

Materials

Dual functional PEG (NH_2-PEG-COOH, Mw = 2000) was from Shanghai Yanyi Biotechnology Corporation (Shanghai, China). FA, FI, N-hydroxysuccinimide (NHS), and 1-ethyl-3-[3-dimethylaminopropyl] carbodiimide hydrochloride (EDC) were purchased from J&K Chemical (Shanghai, China). Ferric chloride hexahydrate ($FeCl_3\cdot 6H_2O$ > 99%), ammonia (25%), branched PEI (Mw = 25 000), triethylamine, acetic anhydride, dimethyl sulfoxid (DMSO), sodium sulfite, and all the other chemicals and solvents were purchased from Aldrich (St. Louis, MO) and used as received. 3-(4,5-dimethylthiazol-2-yl)-2,5-diphenyltetrazolium bromide (MTT) was acquired from Shanghai Sangon Biological Engineering Technology & Services Co., Ltd (Shanghai, China). HeLa cells were from Institute of Biochemistry and Cell Biology, the Chinese Academy of Sciences (Shanghai, China). Dulbecco's modified eagle medium (DMEM), fetal bovine serum (FBS), penicillin, and streptomycin were from Hangzhou Jinuo Biomedical Technology (Hangzhou, China). Water used in all experiments was treated using a Milli-Q Plus 185 water purification system (Millipore, Bedford, MA) with a resistivity higher than 18.2 MΩ.cm.

Preparation of multifunctional FA-functionalized Fe_3O_4 NPs

PEI-coated Fe_3O_4 NPs (Fe_3O_4@PEI NPs) were synthesized *via* a mild reduction route according to the literature[20, 30] with some modifications (Details can be seen in ESI†). PEGylated FA (FA-PEG-COOH) was synthesized, purified and activated according to protocols reported in our previous work.[28, 31] An aqueous solution of the Fe_3O_4@PEI NPs (110 mg, 35 mL) was precipitated *via* an external magnet and re-dispersed in DMSO (20 mL). Then, the activated FA-PEG-COOH (38.5 mg, in 2 mL DMSO) was added dropwise into the above DMSO solution of the Fe_3O_4@PEI NPs and the reaction mixture was vibrated for 3 days. The formed product (Fe_3O_4@PEI-PEG-FA NPs) was collected by an external magnet and washed with DMSO for 3 times to remove excess reactants.

To label the Fe_3O_4@PEI-PEG-FA NPs with a fluorescent dye, FI (3.6 mg, in 4 mL DMSO) was added into the DMSO solution of the Fe_3O_4@PEI-PEG-FA NPs and the mixture was then vibrated in dark for 1 day. Further separation and purification steps were carried out to obtain the Fe_3O_4@PEI-FI-PEG-FA NPs, which were redispersed in water.

Finally, the remaining PEI surface amines on the particle surfaces were acetylated according to the literature.[32, 33] The formed final product (FA-functionalized Fe_3O_4 NPs) was dispersed in water and stored under 4 ^oC before further use. More details can be seen in ESI†.

Characterization techniques

X-ray diffraction (XRD) measurements were carried out using a D/max 2550 PC X-ray diffractometer (Rigaku Cop., Tokyo, Japan) with Cu Kα radiation (λ = 0.154056 nm) at 40 kV and 200 mA and a 2θ scan range of 5-90^o. Fourier transform infrared (FTIR) spectra were recorded on a Nicolet Nexus 670 FTIR spectrometer (Thermo Nicolet Corporation, Madison, WI). Samples were dried and mixed with grounded KBr crystals and pressed as pellets before measurements. Thermal gravimetric analysis (TGA) was performed using a TG 209 F1 (NETZSCH Instruments Co., Ltd., Selb/Bavaria, Germany) thermal gravimetric analyzer in N_2 atmosphere at a heating rate of 20 ^oC/min. Hysteresis loop was measured with a Lakeshore 7407 vibrating sample magnetometer (VSM, Westerville, OH). ^1H NMR spectra were collected using a Bruker AV400 nuclear magnetic resonance spectrometer. D_2O was used as a solvent to dissolve samples prior to measurements. UV-vis spectra were collected using Lambda 25 UV-vis spectrophotometer (Perkin Elmer, Boston, MA), and samples dispersed in water were measured. Fluorescent emission spectrum was collected using a FluoroMax 4 fluorometer (HORIBA Scientific, Edison, NJ). The sample was dispersed in water (0.1 mg/mL) before measurements. The excitation wavelength was set at 490 nm and the fluorescence emission was collected from 500 to 600 nm. Both the excitation and emission slit openings were set at 2 nm. Zeta potential and hydrodynamic size were measured using a Malvern Zetasizer Nano ZS model ZEN3600 (Worcestershire, U.K.) with a standard 633 nm laser. Transmission electron microscopy (TEM) imaging was carried out using a JEOL 2010F analytical electron microscope (JEOL, Tokyo, Japan) with an accelerating voltage of 200 kV. Samples were prepared by deposition of a dilute particle solution (7 μL) onto a carbon-coated copper grid and dried in air prior to analysis. The Fe concentration of the particles dispersed in water or phosphate buffered saline (PBS) was determined by a Leeman Prodigy inductively coupled plasma-optical emission spectroscopy (ICP-OES, Hudson, NH). T_1/T_2 relaxation times of samples was measured by a 0.5 T NMI20-Analyst NMR analyzing and imaging system (Shanghai Niumag Corporation, Shanghai, China). The samples were diluted with water with different Fe concentrations before measurements. The T_1/T_2-weighted images were recorded using a spin-echo imaging sequence with the following parameters: point resolution = 156 mm ×156 mm, section thickness = 0.6 mm, TR = 4000 ms, TE = 60 ms, and number of excitation = 1. The r_1 and r_2 relaxivities were obtained by linearly fitting the inverse T_1 or T_2 relaxation times as a function of Fe concentration.

Hemolysis assay

Fresh human blood stabilized with EDTA was kindly provided by Shanghai First People's Hospital (Shanghai, China) and used with the permission by the ethical committee of Shanghai First People's Hospital. Human red blood cells (HRBCs) were obtained and hemolysis assay was performed according to our previous work.[34-36] Details can be seen in ESI†.

Cell culture

HeLa cells were routinely cultured and passaged in DMEM supplemented with 10% heat-inactivated FBS, 100 U/mL penicillin, and 100 μg/mL streptomycin in a 37 °C incubator with 5% CO_2. The cells cultured in regular DMEM (without FA) expressed high-level FAR (denoted as HeLa-HFAR cells),[37] while the cells cultured in the DMEM containing 2.0 mM free FA expressed low-level FAR (denoted as HeLa-LFAR cells). Unless otherwise stated, HeLa cells were generally denoted as HeLa-HFAR cells.

In vitro cytotoxicity sssay

MTT assay was performed according to the manufacturer's guidelines to evaluate the cytocompatibility of the FA-functionalized Fe_3O_4 NPs. HeLa cells were seeded at a density of 1 × 10^4 cells per well with 200 μL DMEM in a 96-well plate overnight. The medium in each well was then replaced with fresh medium containing FA-functionalized Fe_3O_4 NPs with different Fe concentrations. After incubation at 37 °C and 5% CO_2 for 24 h, MTT solution (20 μL, 5 mg/mL in PBS) was added to each well and the cells were incubated at 37 °C for another 4 h. Then the medium in each well was replaced carefully with 200 μL DMSO, and the absorbance of each well was measured at 570 nm using a Thermo Scientific Multiskan MK3 ELISA reader (Thermo scientific, Hudson, NH). For each sample, 5 parallel wells were used to report the mean and standard deviation. Likewise, after incubation with the FA-functionalized Fe_3O_4 NPs at an Fe concentration range of 0-2.0 mM for 24 h, HeLa cells were rinsed with PBS for 3 times and visualized by phase contrast microscopy (Leica DM IL LED inverted phase contrast microscope). The magnification was set at 200 × for each sample.

Cellular uptake of the FA-functionalized Fe_3O_4 NPs

Flow cytometry and confocal microscopy were used to investigate the cellular uptake of the FA-functionalized Fe_3O_4 NPs. HeLa-HFAR cells (3 × 10^5 cells per well) were seeded in a 12-well tissue culture plate one day before the experiment. The next day, the medium was substituted with fresh medium containing the FA-functionalized Fe_3O_4 NPs with an Fe concentration range of 0-1.0 mM and the cells were cultured at 37 °C and 5% CO_2 for 4 h. The cells were then rinsed with PBS for 3 times, trypsinized, centrifuged, and resuspended in 1 mL PBS. Flow cytometry analysis was performed using a FACSCalibur flow cytometer (Becton Dickinson, Franklin Lakes, NJ). For comparison, HeLa-LFAR cells were treated and analyzed under similar conditions.

The cellular uptake of the FA-functionalized Fe_3O_4 NPs was also evaluated by confocal microscopy (Carl Zeiss LSM 700, Jena, Germany) according to our previous report.[38] HeLa-LFAR cells were also treated and observed in a similar manner for comparison. Details can be found in ESI†.

Targeted MR imaging of cancer cells *in vitro*

HeLa-HFAR or HeLa-LFAR cells were seeded into 6-well plates (3 × 10^6 cells per well) with 2 mL fresh DMEM. The cells were incubated at 37 °C and 5% CO_2 for 24 h to lead the cells to confluence. The medium was then discarded and substituted by fresh DMEM (2 mL) containing PBS (control) or the FA-functionalized Fe_3O_4 NPs with different Fe concentrations. The cells were cultured at 37 °C and 5% CO_2 for additional 4 h. After that, the cells were rinsed with PBS, trypsinized, centrifuged, and resuspended in 1 mL PBS (containing 0.5% agarose) in 2-mL Eppendorf tubes before MR imaging. T_2-weighted MR imaging was performed using a 1.5 T Signa HDxt superconductor clinical MR system (GE Medical Systems, Milwaukee, WI) under the following parameters: point resolution = 156 mm × 156 mm, section thickness = 0.6 mm, TR = 3000 ms, TE = 90.7 ms, and number of excitation = 1.

Targeted MR imaging of a xenografted tumor model *in vivo*

Male 4- to 6-week-old BALB/c nude mice (15-20 g) were provided by Shanghai Slac Laboratory Animal Center (Shanghai, China). All the animal experiments were carried out according to protocols approved by the ethical committee of Shanghai First People's Hospital. To form the tumor model, 2 × 10^6 HeLa cells were subcutaneously injected into the left back of each nude mouse. About one month later, when the xenografted tumor nodules reached a diameter of 1.0-1.5 cm, the mice were anesthetized *via* intraperitoneal injection of pentobarbital sodium (40 mg/kg) and divided into 3 groups: For Group 1, FA-functionalized Fe_3O_4 NPs ([Fe] = 80 mM, 0.1 mL PBS) were intravenously delivered into each mouse *via* the tail vein; For Groups 2 and 3, each mouse was treated with free FA (20 mM, 0.1 mL PBS) *via* intravenous (Group 2) and intratumoral (Group 3) injection, respectively for 30 min before administration of the FA-functionalized Fe_3O_4 NPs with similar dose to Group 1. T_2-weighted MR images of each mouse were obtained using a 1.5 T Signa HDxt superconductor clinical MR system with a custom-built rodent receiver coil (Chenguang Med Tech, Shanghai, China). The parameters were set as follows: slice thickness = 2 mm, TR/TE = 1100/86 ms, FOV = 6 × 6 cm, and matrix = 256 × 160. MR images were obtained before and at 0.5, 1, 2, and 4 h postinjection of the FA-functionalized Fe_3O_4 NPs.

In vivo biodistribution

To explore the *in vivo* biodistribution of the multifunctional FA-functionalized Fe_3O_4 NPs, each tumor-bearing BALB/c nude mouse was intravenously injected with the particles ([Fe] = 80 mM, 0.1 mL PBS) *via* the tail vein. The mice were then sacrificed at different time points (12, 24, 48, and 72 h, respectively) postinjection. The major organs (heart, liver, spleen, lung, and kidney) and tumor were harvested, weighed, and digested in *aqua regia* solution (nitric acid/hydrochloric acid, v/v = 1:3) for 2 days.

After dilution and centrifugation, the Fe content in different organs was quantified by ICP-OES. The tumor-bearing mice without injection were used as control.

Hematology and histology studies

Each tumor-bearing mouse was injected with the FA-functionalized Fe_3O_4 NPs ([Fe] = 80 mM, 0.1 mL PBS) *via* the tail vein. After 10 days, blood samples and the major organs of mice (heart, liver, spleen, lung, and kidney) were harvested for hematology and histology studies. A blood smear was prepared by placing a drop of blood onto a slide and air dried. For histological examinations, the organs were fixed in formaldehyde, paraffin embedded, sectioned, and hematoxylin and eosin (H&E) stained according to protocols reported in the literature.[39] Finally, the blood smears and histological sections were observed under a phase contrast microscope (Leica DM IL LED inverted phase contrast microscope). The magnification of 200 × was set for each sample.

Statistical analysis

One-way ANOVA analysis was carried out to evaluate the significance of the experimental data. A p value of 0.05 was chosen as the significance level, and the data were indicated with (*) for $p < 0.05$, (**) for $p < 0.01$, and (***) for $p < 0.001$, respectively.

Results and discussion

Synthesis and characterization of FA-functionalized Fe_3O_4 NPs

Using a mild reduction method,[20] we synthesized PEI-coated Fe_3O_4 NPs in aqueous solution by reducing Fe^{3+} in the presence of PEI. The PEI-coated Fe_3O_4 NPs (Fe_3O_4@PEI NPs) were then modified with PEGylated FA and FI *via* the PEI amine-mediated covalent conjugation. Subsequent acetylation of the remaining PEI surface amines gave rise to the formation of multifunctional FA-functionalized Fe_3O_4 NPs (Scheme 1).

Various techniques were utilized to characterize the intermediate product and the formed FA-functionalized Fe_3O_4 NPs. For comparison, naked Fe_3O_4 NPs were also formed under similar experimental conditions in the absence of PEI. The crystal structure of the formed Fe_3O_4@PEI NPs was characterized by XRD (Fig. S1, ESI†). Clearly, the XRD pattern of the Fe_3O_4@PEI NPs (Fig. S1, Curve a) is identical to that of naked Fe_3O_4 NPs (Fig. S1, Curve b), and the peaks at 2θ of 30.1, 35.5, 43.0, 53.4, 57.0, 62.6, and 74.8° well match the [220], [311], [400], [422], [511], [440], and [533] planes of magnetite, respectively.[40, 41] The broad peak at 22.5° for the Fe_3O_4@PEI NPs is likely to be attributed to the PEI coating.

FTIR spectrometry was next used to qualitatively demonstrate the PEI coating on the surface of Fe_3O_4 NPs (Fig. S2, ESI†). We can see that naked Fe_3O_4 NPs exhibit weak bands at 3450 and 1630 cm^{-1} that can be assigned to the O-H stretching and bending vibrations of physically adsorbed H_2O and the surface -OH groups of the particles (Fig. S2, Curve a). However, due to the introduced PEI amines, the Fe_3O_4@PEI NPs show very strong bands at 3450 and 1630 cm^{-1} in the spectrum (Fig. S2b). What's more, the strong absorption bands at 2930 and 2850 cm^{-1} in the spectrum of the Fe_3O_4@PEI NPs could be assigned to the PEI -CH_2- groups and the band at 1090 cm^{-1} can be assigned to the stretching vibration of the C-N bond. In addition, the naked Fe_3O_4 NPs have a very large hydrodynamic size (1177.6 nm) due to the absence of PEI stabilization with a surface potential of -9.0 mV (Table S1, ESI†). In sharp contrast, the Fe_3O_4@PEI NPs display a much smaller size (164.2 nm) and a quite positive surface potential (+52.8 mV). These results suggest that PEI has been successfully coated onto the surface of the Fe_3O_4 NPs.

To quantify the degree of PEI coating onto the particle surface, TGA was carried out (Fig. S3, ESI†). It is obvious that the Fe_3O_4@PEI NPs have a weight of 88.53% at the temperature as high as 700 °C (Fig. S3, Curve b). Due to the fact that naked Fe_3O_4 NPs do not show any significant weight loss (Fig. S3, Curve a),[24, 25] the percentage of PEI coating was calculated to be 11.47%.

The morphology of the prepared Fe_3O_4@PEI NPs was observed by TEM (Fig. S4a, ESI†). It can be seen that the particles have a quite uniform spherical or quasi-spherical shape with an average size of 9.0 nm (Fig. S4b, ESI†). The magnetic property of the Fe_3O_4@PEI NPs at room temperature was evaluated by VSM (Fig. S4c, ESI†). The lack of a hysteresis loop suggests the superparamagnetic nature of the NPs. The saturated magnetization (M_s) was calculated to be 53.6 emu g^{-1}, which is lower than the bulk magnetite (92 emu g^{-1}) reported in the literature.[42] The decreased M_s is normally considered to be due to the polymer coating on the particle surface.[43] Shown in the inset of Fig. S4c is the digital picture of the aqueous suspension of the Fe_3O_4@PEI NPs before and after exposed to a magnetic field. Clearly, the particles can be collected by the magnet, suggesting their good magnetic properties.

To investigate the potential to utilize the Fe_3O_4@PEI NPs for MR imaging applications, we measured the T_1 and T_2 values of the Fe_3O_4@PEI NPs with different Fe concentrations and calculated the longitudinal (r_1) and transverse (r_2) relaxivity (Fig. S5, ESI†). The r_1 and r_2 relaxivities were calculated to be 29.49 and 461.29 $mM^{-1}s^{-1}$, respectively, much higher than those of other Fe_3O_4 NPs used for either T_1 or T_2 MR imaging.[44, 45] A recent study has shown that the r_2 relaxivity of PEI-coated Fe_3O_4 NPs could be significantly affected by the PEI concentration during the particles synthesis.[46] The r_2 relaxivity of the NPs prepared at 0.05 wt% PEI (227.6 $mM^{-1}s^{-1}$) was much larger than that of the NPs prepared at 0.02 wt% PEI (45.0 $mM^{-1}s^{-1}$) and 0.08 wt% PEI (29.5 $mM^{-1}s^{-1}$). It seems that the formed particles with appropriate size and aggregation state have a higher r_2 value, in agreement with the literature.[47, 48] In addition, the employed mild synthesis method here may allow for the generation of particles with super high magnetic dipole interactions, which is extremely powerful to generate strong local magnetic field. This substantially affects the relaxation process of water protons around the particles and simultaneously shortens the T_2 relaxation time and improves the MR contrast enhancement.[49, 50] Overall, the mechanism related to the ultrahigh r_2 relaxivity is still not very clear and needs to be further explored. In any case, the good magnetic properties and much higher r_2 relaxivity of the Fe_3O_4@PEI NPs than those of the previously reported PEI-coated Fe_3O_4 NPs[25, 28] are essential for their further sensitive MR imaging applications.

To afford the Fe_3O_4 NPs with targeting specificity to cancer cells, PEGylated FA was then modified on the surface of the particles. The structure of the PEGylated FA was firstly characterized by ^1H NMR (Fig. S6, ESI†). Similar to our previous study,[28] the obvious peaks at 6.63, 7.51, and 8.65 ppm in the spectrum can be assigned to the aromatic protons of FA, and the peak at 3.5 ppm can be assigned to the PEG $-CH_2-$ protons. This suggests that FA has been successfully linked to the PEG. The average number of FA conjugated to each PEG was calculated to be 0.77 based on NMR integration. The conjugation of PEGylated FA onto the surface of the Fe_3O_4@PEI NPs was first qualitatively confirmed by FTIR (Fig. S2, Curve c). Compared with the Fe_3O_4@PEI NPs (Fig. S2, Curve b) and free FA (Fig. S2, Curve d), we can see that the Fe_3O_4@PEI-PEG-FA NPs display an intense peak at 1405 cm^{-1} that can be assigned to the aromatic ring stretch of the pteridine ring and ρ-amino benzoic acid moieties of FA,[37] suggesting the success in the conjugation of PEGylated FA onto the surface of the Fe_3O_4@PEI NPs. TGA was used to quantitatively characterize the modification degree of the PEGylated FA onto the particle surfaces (Fig. S3, Curve c). With the weight loss of the Fe_3O_4@PEI-PEG-FA NPs estimated to be 23.92% at 700 ^oC and the known weight loss of the Fe_3O_4@PEI NPs (11.47%) at the same temperature, the percentage of the PEGylated FA modified onto the particle surfaces was calculated to be 12.45%.

The formed Fe_3O_4@PEI-PEG-FA NPs were then conjugated with FI *via* a thiourea bond to render the particles with fluorescence tracking property. UV-vis spectroscopy was used to verify the modification of FI onto the particle surfaces (Fig. S7a, ESI†). Obviously, an absorption peak at 505 nm appearing in the spectrum of the Fe_3O_4@PEI-FI-PEG-FA NPs can be assigned to the typical FI absorption. In contrast, the Fe_3O_4@PEI-PEG-FA NPs without FI modification do not exhibit the same absorption feature. Our results clearly suggest the successful FI conjugation onto the Fe_3O_4@PEI-PEG-FA NPs, in agreement with the literature.[51] In addition, the Fe_3O_4@PEI-FI-PEG-FA NPs displaying an obvious fluorescent emission peak at 522 nm do not seem to have any FI fluorescence quenching effect (Fig. S7b, ESI†).

The remaining PEI amines on the surface of the Fe_3O_4@PEI-FI-PEG-FA NPs were subjected to acetylation to alleviate the positive surface charge of the particles. Zeta potential measurements reveal that the final product of the Fe_3O_4@PEI.Ac-FI-PEG-FA NPs (FA-functionalized Fe_3O_4 NPs) displays a surface potential of +24.2 mV, which is much lower than the nonacetylated particles (+39.4 mV, Table S1). It should be noted that the acetylation reaction is unable to fully neutralize the positive surface charge of the particles because some PEI amines played a role to stabilize the Fe_3O_4 NPs are unable to be fully acetylated, correlating well with our previous reports.[28, 36] The hydrodynamic size of the FA-functionalized Fe_3O_4 NPs dispersed in different aqueous media for 2 weeks was also measured to evaluate their colloidal stability (Fig. S8, ESI†). Clearly, regardless of the used medium of water, PBS or cell culture medium, the hydrodynamic size of the FA-functionalized Fe_3O_4 NPs do not show significant changes, indicating their good colloidal stability. What's more, the colloidal stability of the FA-functionalized Fe_3O_4 NPs in water, PBS, or cell culture medium was also occasionally checked over a period of one month. The particles are quite colloidally stable and no precipitates were seen over the one month period (Fig. S8 inset, ESI†).

The size and morphology of the formed FA-functionalized Fe_3O_4 NPs were observed by TEM (Fig. 1). It is obvious that the particles possess a spherical or quasi-spherical shape and display a relatively narrow size distribution with a mean diameter of 8.9 ± 2.1 nm (Fig. 1a and b). It is interesting to note that the measured size by TEM is much smaller than the hydrodynamic size (310.5 nm) measured by dynamic light scattering (DLS, using Zetasizer) in water. This can be due to the fact that TEM is used to measure a single Fe_3O_4 core particle, while DLS is used to measure the size of large clusters of particles in aqueous solution that may be composed of many single particles.[28, 29, 52, 53] High-resolution TEM image reveals that the formed particles are crystalline, and lattices of Fe_3O_4 crystals can be observed (Fig. 1c), although the crystalline lattice structure in some particles is not prominent. The crystalline nature of the FA-functionalized Fe_3O_4 NPs was also proven using selected area electron diffraction (SAED, Fig. 1d). The lack of clear crystal lattice image and SAED pattern may suggest that the Fe_3O_4 NPs synthesized *via* a mild reduction route is not highly crystalline.

We next performed both T_1- and T_2-weighted MR imaging of the FA-functionalized Fe_3O_4 NPs dispersed in water (Fig. 2a). Clearly, the particles are able to increase the MR signal intensity in T_1-weighted MR images and decrease the MR signal intensity in the T_2-weighted MR images with the Fe concentration. A linear fitting of the relaxation rates ($1/T_1$ and $1/T_2$) as a function of Fe concentration (Fig. 2b) was used to calculate the r_1 and r_2 relaxivities to be 35.69 and 475.92 $mM^{-1}s^{-1}$, respectively. The relaxivity data are quite similar to those of the Fe_3O_4@PEI NPs, suggesting that the further multi-step modification does not cause any appreciable changes in the relaxivity of the particles. The ultrahigh r_1 and r_2 relaxivities of the synthesized FA-functionalized Fe_3O_4 NPs may be due to the nature of the mild reduction synthesis method, allowing for the generation of particles with super high magnetic dipole interactions. The ultrahigh r_2 value and the great r_2/r_1 ratio of 13.33 suggest that the developed FA-functionalized Fe_3O_4 NPs have a great potential to be used as favorable contrast agents for T_2 MR imaging applications. It is notable that the FA-functionalized Fe_3O_4 NPs display a much higher r_2 relaxivity than the hydrothermally synthesized Fe_3O_4 NPs reported in the literature,[28] which is very important for highly sensitive MR imaging of biological systems.

Hemolysis assay

Hemocompatibility is one important issue to be considered before *in vivo* applications of the FA-functionalized Fe_3O_4 NPs. Hemolysis assay was conducted to assess the hemocompatibility of the FA-functionalized Fe_3O_4 NPs according to protocols reported in the literature (Fig. S9, ESI†).[36, 54] As shown in the inset of Fig. S9, no obvious hemolysis effect is visually observed in the studied Fe concentration range of the particles, which is similar to the PBS control. In sharp contrast, the HRBCs exposed to water (positive control) display an obvious hemolysis activity. Quantitative analysis *via* UV-vis spectroscopic measurement of the absorbance of the supernatant at 541 nm (hemoglobin) reveals that the hemolysis percentage of the FA-functionalized Fe_3O_4 NPs is less than 1.23% even at a high Fe concentration of 8.0 mM (Fig. S9). This result suggests that the FA-functionalized Fe_3O_4

NPs have a negligible hemolytic activity.

***In vitro* cytotoxicity assay**

The cytotoxicity of the formed FA-functionalized Fe_3O_4 NPs was then evaluated by MTT cell viability assay (Fig. 3a). Clearly, the cell viability is higher than 87% after treatment with the particles in the Fe concentration range of 0.2-1.5 mM. At a Fe concentration of 2.0 mM, the cell viability stilled reached 74.6%. These results suggest that the FA-functionalized Fe_3O_4 NPs are cytocompatible in a studied concentration range.

The cytocompatibility of the FA-functionalized Fe_3O_4 NPs was further verified by visualization of the morphology of the HeLa cells treated with the particles at different Fe concentrations for 24 h (Fig. S10, ESI†). It can be seen that the cells treated with the FA-functionalized Fe_3O_4 NPs at the Fe concentrations of 0.2, 0.4, 0.6, 0.8, and 1.0 mM do not display any significant morphological changes when compared with the control cells treated with PBS (Fig. S10a-f). In addition, at the Fe concentration up to 1.5 and 2.0 mM, a portion of cells started to become detached, indicating the death of cells (Fig. S10g and h). These cell morphology observation results corroborated the above MTT assay data, confirming the good cytocompatibility of the FA-functionalized Fe_3O_4 NPs in the studied concentration range.

Targeted cellular uptake of the FA-functionalized Fe_3O_4 NPs

To render the formed Fe_3O_4 NPs with targeting specificity, PEGylated FA was modified onto the particle surfaces, since FA is a well known targeting ligand that can target several FAR-overexpressing human carcinomas including breast, ovary, endometrium, kidney, lung, head and neck, brain, and myeloid cancers.[55-57] We next explored the targeting specificity of the FA-functionalized Fe_3O_4 NPs *via* flow cytometry (Fig. S11, ESI†). Obviously, HeLa-HFAR cells treated with the FA-functionalized Fe_3O_4 NPs exhibit much higher FI-related fluorescence signal intensity than the HeLa-LFAR cells under similar experimental conditions, especially at the Fe concentration of 0.4 mM. Quantitative fluorescence measurements were also used to evaluate the cellular uptake of the FA-functionalized Fe_3O_4 NPs by the two types of HeLa cells (Fig. 3b). Clearly, HeLa-HFAR cells treated with the FA-functionalized Fe_3O_4 NPs display higher fluorescence intensity than HeLa-LFAR cells treated at the same Fe concentrations. The enhanced cellular uptake of the particles by the HeLa-HFAR cells should be attributed to the attached FA ligands that can render the particles with targeting specificity to the FAR-overexpressing cancer cells *via* ligand-receptor interaction.[37, 58]

The modified FI moiety onto the surface of the FA-functionalized Fe_3O_4 NPs also affords the the particles to be visualized *via* confocal microscopic imaging once the particles are uptaken by cells (Fig. 4). An intensive fluorescence signal can be seen on the surface and in the cytoplasm of the HeLa-HFAR cells after treated with the FA-functionalized Fe_3O_4 NPs ([Fe] = 0.4 mM) for 4 h (Fig. 4b). In contrast, only slight fluorescence signals were observed in the HeLa-LFAR cells under similar experimental conditions (Fig. 4c), which is comparable to the control cells treated with PBS (Fig. 4a). These results demonstrate the effective targeting specificity of the FA-functionalized Fe_3O_4 NPs to HeLa-HFAR cells *via* FAR-mediated targeting pathway.

***In vitro* targeted MR imaging of cancer cells**

Next, we investigated the possibility to use the FA-functionalized Fe_3O_4 NPs as a nanoprobe for targeted cancer cell MR imaging *in vitro* (Fig. 5). In the T_2-weighted MR images (Fig. 5a), both HeLa-HFAR and HeLa-LFAR cells showed gradually reduced MR signal intensity with the Fe concentration (from 0.1 to 0.4 mM). However, the MR signal decreasing trend for HeLa-HFAR cells is much more prominent than that for HeLa-LFAR cells treated with the particles at the same Fe concentrations. A quantitative T_2 MR signal intensity analysis (Fig. 5b) further show that the FA-functionalized Fe_3O_4 NPs are capable to decrease the MR signal intensity of both HeLa-HFAR and HeLa-LFAR cells due to the cellular uptake of the particles. Similarly, the signal intensity of the HeLa-HFAR cells is obviously lower than that of the HeLa-LFAR cells at the same Fe concentrations. Our results further highlighted the role played by the attached FA ligands that can make the particles actively target to FAR-overexpressing HeLa cells *via* a FAR-mediated manner, enabling effective targeted MR imaging of cancer cells *in vitro*.

***In vivo* targeted MR imaging of a xenografted tumor model**

To further validate the potential to use the FA-functionalized Fe_3O_4 NPs for targeted MR imaging of tumors, the HeLa tumor-bearing mice were intravenously injected with the particles and the mice were MR scanned at different time points postinjection. For comparison, mice were also intravenously (Group 2) or intratumorally (Group 3) injected with free FA (20 mM, 0.1 mL PBS) for 30 min to block the FAR expression before the administration of the FA-functionalized Fe_3O_4 NPs. The T_2-weighted colored tumor MR images (Fig. 6a) reveal that the tumor MR signal for all groups gradually decreases from the time before injection to 1 h postinjection, which is likely due to the fact that the particles can be gradually accumulated into the tumor sites. From 2 to 4 h postinjetcion, the particles started to be further metabolized to diffuse to other tissues or organs from the tumors, so the tumor MR signal became gradually recovered. Importantly, the tumor MR signal of mouse in Group 1 at 1 h post injection is much lower than those in Groups 2 and 3. This suggests that the developed FA-functionalized Fe_3O_4 NPs enables effective targeted MR imaging of tumors *via* an FAR-mediated targeting pathway. Quantitative analysis of the tumor MR signal intensity also revealed the exact similar trend of MR signal intensity change (Fig. 6b). It is interesting to note that the ultrahigh r_2 relaxivity renders the FA-functionalized Fe_3O_4 NPs with significantly improved *in vivo* MR imaging performance. The tumor MR signal intensity dropped to 48.6% at 1 h postinjection. This decreasing trend is much higher than that of the FA-functionalized Fe_3O_4 NPs synthesized *via* controlled co-precipitation route (72.7% at 4 h postinjection) or the FA-modified magnetic micelles (72.6% at 1 h postinjection).[59, 60] In general, NPs can be efficiently taken up by the reticuloendothelial system (RES) after they are injected into the mice through intravenous injection, and only limited particles can reach the tumor sites. In our case, due to the surface PEGylation of the particles, a portion of the developed FA-functionalized Fe_3O_4 NPs are able to escape from the RES, and be accumulated in the tumor tissue *via* both passive enhanced permeability and retention

(EPR) effect and active FAR-mediated targeting pathway, allowing for effective tumor MR imaging. On the other hand, the PEGylation modification may hinder the formation of protein corona onto the surface of particles, ensuring the effective targeting specificity to the tumor site *in vivo*.[61]

In vivo biodistribution

For targeted tumor MR imaging, it is necessary to explore the biodistribution behavior of the formed FA-functionalized Fe_3O_4 NPs. ICP-OES data (Fig. S12, ESI†) reveal that only a relatively small amount of Fe is taken up in the heart, lung, kidney, and tumor at the studied time points, while a majority of Fe is taken up in the liver and spleen at 12 to 24 h postinjection with peak uptake of 405.64 and 2303.85 μg/g, respectively. The rapid accumulation of the particles in the liver and spleen and relatively slow excretion of the particles are quite typical due to the clearance effect of the RES in these organs.[62] After 24 h, the Fe content in the liver and spleen started to decrease as time passed by, and the liver and spleen uptake of Fe is 241.74 and 1054.38 μg/g, respectively at 72 h postinjection. Notably, the positive surface potential of the particles does not render the particles with improved organ uptake due to the surface PEGylation modification, in agreement with the literature.[28] Our results indicate that the FA-functionalized Fe_3O_4 NPs are able to be slowly excreted from the living body and potentially do not generate *in vivo* toxicity.

Hematology and histology examinations

Hematology and histology studies were carried out to evaluate the potential *in vivo* toxicity of the FA-functionalized Fe_3O_4 NPs. As shown in Fig. 7, blood smears reveal that the number and shape of blood cells for mice treated with the particles are normal and no inflammatory response is observed when compared with the control mice. Similarly, the structure and morphology of all organs of the mice injected with the particles are all similar to those of the corresponding organs of the control mice and no apparent tissue or cellular damage was observed. This suggests that the injected FA-functionalized Fe_3O_4 NPs do not display any appreciable *in vivo* toxicity to the mice, hence having a great potential to be used as a nanoprobe for targeted tumor MR imaging applications.

Conclusions

To conclude, we developed a convenient mild reduction approach to forming FA-functionalized Fe_3O_4 NPs with an ultrahigh r_2 relaxivity. The PEI coating onto the surface of the particles enabled effective conjugation of PEGylated FA and FI *via* PEI amine-enabled conjugation chemistry. The formed multifunctional particles displayed good water dispersibility, colloidal stability, hemocompatibility and cytocompatibility in the studied concentration range, and excellent targeting specificity to FAR-overexpressing cancer cells. More importantly, the developed FA-functionalized Fe_3O_4 NPs were able to be used as a multifunctional nanoprobe for targeted MR imaging of cancer cells *in vitro* and the xenografted tumor model *in vivo*. Taking into consideration of the good *in vivo* organ compatibility, the developed FA-functionalized Fe_3O_4 NPs may be used as a promising nanoprobe for targeted MR imaging of different types of FAR-overexpressing tumors.

Acknowledgements

This research is financially supported by the National Natural Science Foundation of China (21273032, 81101150, 81341050, and 81371623), the Fund of the Science and Technology Commission of Shanghai Municipality (12520705500), the Sino-German Center for Research Promotion (GZ899), and the Program for Professor of Special Appointment (Eastern Scholar) at Shanghai Institutions of Higher Learning.

Notes and references

[a] *College of Chemistry, Chemical Engineering and Biotechnology, Donghua University, Shanghai 201620, People's Republic of China E-mail: xshi@dhu.edu.cn (X. Shi), mwshen@dhu.edu.cn (M. Shen)*
[b] *Department of Radiology, Shanghai First People's Hospital, School of Medicine, Shanghai Jiaotong University, Shanghai 200080, P. R. China*
[c] *State Key Laboratory of Modification of Chemical Fibers and Polymer Materials, College of Materials Science and Engineering, Donghua University, Shanghai 201620, People's Republic of China*
[d] *Department of Cardiographic Ultrason, Shanghai First People's Hospital, School of Medicine, Shanghai Jiaotong University, Shanghai 200080, P. R. China*
E-mail: syp2101@hotmail.com (Y. Sun)
[1] *Jingchao Li, Yong Hu and Jia Yang contributed equally to this work.*

† **Electronic supplementary information (ESI) available**: additional experimental details and results.

1. J. Zhao, J. Fei, C. Du, W. Cui, H. Ma and J. Li, *Chem. Commun.*, 2013, **49**, 10733-10735.
2. J. Li, Y. Hu, J. Yang, P. Wei, W. Sun, M. Shen, G. Zhang and X. Shi, *Biomaterials*, 2015, **38**, 10-21.
3. B. Zhou, L. Zheng, C. Peng, D. Li, J. Li, S. Wen, M. Shen, G. Zhang and X. Shi, *ACS Appl. Mater. Interfaces*, 2014, **6**, 17190-17199.
4. C. Du, J. Zhao, J. Fei, Y. Cui and J. Li, *Adv. Healthcare Mater.*, 2013, **2**, 1246-1251.
5. L. Gao, J. Fei, J. Zhao, H. Li, Y. Cui and J. Li, *ACS Nano*, 2012, **6**, 8030-8040.
6. S. Laurent, D. Forge, M. Port, A. Roch, C. Robic, L. Vander Elst and R. N. Muller, *Chem. Rev.*, 2008, **108**, 2064-2110.
7. L.-h. Shen, J.-f. Bao, D. Wang, Y.-x. Wang, Z.-w. Chen, L. Ren, X. Zhou, X.-b. Ke, M. Chen and A.-q. Yang, *Nanoscale*, 2013, **5**, 2133-2141.
8. J. Yang, Y. Luo, Y. Xu, J. Li, Z. Zhang, H. Wang, M. Shen, X. Shi and G. Zhang, *ACS Appl. Mater. Interfaces*, 2015, **7**, 5420-5428.
9. A. G. Roca, J. F. Marco, M. d. P. Morales and C. J. Serna, *J. Phys. Chem. B*, 2007, **111**, 18577-18584.
10. H. Lee, E. Lee, D. K. Kim, N. K. Jang, Y. Y. Jeong and S. Jon, *J. Am. Chem. Soc.* , 2006, **128**, 7383-7389.
11. Y.-M. Huh, Y.-w. Jun, H.-T. Song, S. Kim, J.-s. Choi, J.-H. Lee, S. Yoon, K.-S. Kim, J.-S. Shin and J.-S. Suh, *J. Am. Chem. Soc.*, 2005, **127**, 12387-12391.
12. S. Mohapatra, S. K. Mallick, T. K. Maiti, S. K. Ghosh and P. Pramanik, *Nanotechnology*, 2007, **18**, 385102.
13. E. Taboada, E. Rodríguez, A. Roig, J. Oró, A. Roch and R. N. Muller, *Langmuir*, 2007, **23**, 4583-4588.
14. U. I. Tromsdorf, O. T. Bruns, S. C. Salmen, U. Beisiegel and H. Weller, *Nano Lett.*, 2009, **9**, 4434-4440.
15. L. Zeng, W. Ren, J. Zheng, P. Cui and A. Wu, *Phys. Chem. Chem. Phys.*, 2012, **14**, 2631-2636.
16. S. H. Wang, X. Shi, M. Van Antwerp, Z. Cao, S. D. Swanson, X. Bi and J. R. Baker, *Adv. Funct. Mater.*, 2007, **17**, 3043-3050.
17. J. Xie, K. Chen, H.-Y. Lee, C. Xu, A. R. Hsu, S. Peng, X. Chen and S. Sun, *J. Am. Chem. Soc.*, 2008, **130**, 7542-7543.
18. H. Yang, Y. Zhuang, Y. Sun, A. Dai, X. Shi, D. Wu, F. Li, H. Hu and S. Yang, *Biomaterials*, 2011, **32**, 4584-4593.

19. C. Y. Haw, F. Mohamed, C. H. Chia, S. Radiman, S. Zakaria, N. M. Huang and H. N. Lim, *Ceram Int.*, 2010, **36**, 1417-1422.
20. J. Hong, D. Xu, J. Yu, P. Gong, H. Ma and S. Yao, *Nanotechnology*, 2007, **18**, 135608.
21. D. Liu, J. Shi, L. Tong, X. Ren, Q. Li and H. Yang, *J. Nanopart. Res.*, 2012, **14**, 1-7.
22. X. Sun, F. Liu, L. Sun, Q. Wang and Y. Ding, *J. Inorg. Organomet Polym.*, 2012, **22**, 311-315.
23. M. Bagherzadeh, M. M. Haghdoost, F. M. Moghaddam, B. K. Foroushani, S. Saryazdi and E. Payab, *J. Coord. Chem.*, 2013, **66**, 3025-3036.
24. M. Shen, H. Cai, X. Wang, X. Cao, K. Li, S. H. Wang, R. Guo, L. Zheng, G. Zhang and X. Shi, *Nanotechnology*, 2012, **23**, 105601.
25. H. Cai, X. An, J. Cui, J. Li, S. Wen, K. Li, M. Shen, L. Zheng, G. Zhang and X. Shi, *ACS Appl. Mater. Interfaces*, 2013, **5**, 1722-1731.
26. S. Wen, K. Li, H. Cai, Q. Chen, M. Shen, Y. Huang, C. Peng, W. Hou, M. Zhu and G. Zhang, *Biomaterials*, 2013, **34**, 1570-1580.
27. C. Peng, L. Zheng, Q. Chen, M. Shen, R. Guo, H. Wang, X. Cao, G. Zhang and X. Shi, *Biomaterials*, 2012, **33**, 1107-1119.
28. J. Li, L. Zheng, H. Cai, W. Sun, M. Shen, G. Zhang and X. Shi, *Biomaterials*, 2013, **34**, 8382-8392.
29. J. Li, Y. He, W. Sun, Y. Luo, H. Cai, Y. Pan, M. Shen, J. Xia and X. Shi, *Biomaterials*, 2014, **25**, 3666-3677.
30. Y. Hu, J. Li, J. Yang, P. Wei, Y. Luo, L. Ding, W. Sun, G. Zhang, X. Shi and M. Shen, *Biomater. Sci.*, 2015, **3**, 721-732.
31. Q. Chen, K. Li, S. Wen, H. Liu, C. Peng, H. Cai, M. Shen, G. Zhang and X. Shi, *Biomaterials*, 2013, **34**, 5200-5209.
32. H. Liu, Y. Xu, S. Wen, Q. Chen, L. Zheng, M. Shen, J. Zhao, G. Zhang and X. Shi, *Chem. Eur. J*, 2013, **19**, 6409-6416.
33. C. Peng, H. Wang, R. Guo, M. Shen, X. Cao, M. Zhu, G. Zhang and X. Shi, *J. Appl. Polym. Sci.*, 2011, **119**, 1673-1682.
34. Y. Zhao, S. Wang, Q. Guo, M. Shen and X. Shi, *J. Appl. Polym. Sci.*, 2013, **127**, 4825-4832.
35. H. Cai, K. Li, M. Shen, S. Wen, Y. Luo, C. Peng, G. Zhang and X. Shi, *J. Mater. Chem.*, 2012, **22**, 15110-15120.
36. J. Li, L. Zheng, H. Cai, W. Sun, M. Shen, G. Zhang and X. Shi, *ACS Appl. Mater. Interfaces*, 2013, **5**, 10357-10366.
37. C. Sun, R. Sze and M. Zhang, *J. Biomed. Mater. Res. Part A*, 2006, **78**, 550-557.
38. S. Wang, Y. Wu, R. Guo, Y. Huang, S. Wen, M. Shen, J. Wang and X. Shi, *Langmuir*, 2013, **29**, 5030-5036.
39. C. Peng, J. Qin, B. Zhou, Q. Chen, M. Shen, M. Zhu, X. Lu and X. Shi, *Polym. Chem.*, 2013, **4**, 4412-4424.
40. S. Ge, X. Shi, K. Sun, C. Li, C. Uher, J. R. Baker Jr, M. M. Banaszak Holl and B. G. Orr, *J. Phys. Chem. C*, 2009, **113**, 13593-13599.
41. G. Liu, H. Wu, H. Zheng, L. Tang, H. Hu, H. Yang and S. Yang, *J. Mater. Sci.*, 2011, **46**, 5959-5968.
42. S. Chikazumi, *Physics of Magnetism*, Wiley, New York, 1964.
43. J. Wang, M. Yao, G. Xu, P. Cui and J. Zhao, *Mater. Chem. Phys.*, 2009, **113**, 6-9.
44. X. Shi, S. H. Wang, S. D. Swanson, S. Ge, Z. Cao, M. E. Van Antwerp, K. J. Landmark and J. R. Baker, *Adv. Mater.*, 2008, **20**, 1671-1678.
45. F. Hu, Q. Jia, Y. Li and M. Gao, *Nanotechnology*, 2011, **22**, 245604.
46. M. A. Do, G. J. Yoon, J. H. Yeum, M. Han, Y. Chang and J. H. Choi, *Colloids Surf., B*, 2014, **122**, 752-759.
47. H. Ai, C. Flask, B. Weinberg, X. T. Shuai, M. D. Pagel, D. Farrell, J. Duerk and J. Gao, *Adv. Mater.*, 2005, **17**, 1949-1952.
48. M. Wu, D. Zhang, Y. Zeng, L. Wu, X. Liu and J. Liu, *Nanotechnology*, 2015, **26**, 115102.
49. D. Mitchell, D. Burk Jr, S. Vinitski and M. Rifkin, *Am. J. Roentgenol.*, 1987, **149**, 831-837.
50. S. J. Erickson, R. W. Prost and M. Timins, *Radiology*, 1993, **188**, 23-25.
51. S. Wen, H. Liu, H. Cai, M. Shen and X. Shi, *Adv. Healthcare Mater.*, 2013, **2**, 1267-1276.
52. H. Liu, Y. Xu, S. Wen, J. Zhu, L. Zheng, M. Shen, J. Zhao, G. Zhang and X. Shi, *Polym. Chem.*, 2013, **4**, 1788-1795.
53. M. P. Calatayud, B. Sanz, V. Raffa, C. Riggio, M. R. Ibarra and G. F. Goya, *Biomaterials*, 2014, **35**, 6389-6399.
54. C. Peng, K. Li, X. Cao, T. Xiao, W. Hon, L. Zheng, R. Guo, M. Shen, G. Zhang and X. Shi, *Nanoscale*, 2012, **4**, 6768-6778.
55. I. G. Campbell, T. A. Jones, W. D. Foulkes and J. Trowsdale, *Cancer Res.*, 1991, **51**, 5329-5338.
56. J. F. Ross, P. K. Chaudhuri and M. Ratnam, *Cancer*, 1994, **73**, 2432-2443.
57. D. Weitman, R. H. Lark, L. R. Coney, D. W. Fort, V. Frasca, V. R. Surawski and B. A. Kamen, *Cancer Res.*, 1992, **52**, 3396-3401.
58. F.-H. Chen, L.-M. Zhang, Q.-T. Chen, Y. Zhang and Z.-J. Zhang, *Chem. Commun.*, 2010, **46**, 8633-8635.
59. Q. Jiang, S. Zheng, R. Hong, S. Deng, L. Guo, R. Hu, B. Gao, M. Huang, L. Cheng and G. Liu, *Appl.Surf. Sci.*, 2014, **307**, 224-233.
60. H. Li, K. Yan, Y. Shang, L. Shrestha, R. Liao, F. Liu, P. Li, H. Xu, Z. Xu and P. K. Chu, *Acta Biomater.*, 2015, **15**, 117-126.
61. A. Salvati, A. S. Pitek, M. P. Monopoli, K. Prapainop, F. B. Bombelli, D. R. Hristov, P. M. Kelly, C. Åberg, E. Mahon and K. A. Dawson, *Nat. Nanotechnol.*, 2013, **8**, 137-143.
62. H. Hu, A. Dai, J. Sun, X. Li, F. Gao, L. Wu, Y. Fang, H. Yang, L. An and H. Wu, *Nanoscale*, 2013, **5**, 10447-10454.

Figure captions

Scheme 1. Schematic representation of the synthesis of FA-functionalized Fe_3O_4 NPs. TEA and Ac_2O represent triethylamine and acetic anhydride, respectively.

Fig. 1. TEM micrograph (a), size distribution histogram (b), high-resolution TEM image (c), and selected area electron diffraction pattern (d) of the FA-functionalized Fe_3O_4 NPs.

Fig. 2. Color T_1 and T_2-weighted MR images (a) and linear fitting of $1/T_1$ and $1/T_2$ (b) of the FA-functionalized Fe_3O_4 NPs at different Fe concentrations. The color bar from red to blue indicates the gradual decrease of MR signal intensity.

Fig. 3. (a) MTT assay of HeLa cell viability after treatment with the FA-functionalized Fe_3O_4 NPs at different Fe concentrations for 24 h. (b) The mean fluorescence of the HeLa-HFAR and HeLa-LFAR cells after treatment with the FA-functionalized Fe_3O_4 NPs at different Fe concentrations for 4 h.

Fig. 4. Confocal microscopic images of the HeLa-HFAR (b) and HeLa-LFAR (c) cells after treated with the FA-functionalized Fe_3O_4 NPs at a Fe concentration of 0.4 mM for 4 h. The HeLa-HFAR cells treated with PBS were used as control (a).

Fig. 5. T_2-weighted MR images (a) and MR signal intensity (b) of HeLa-HFAR and HeLa-LFAR cells after treated with the FA-functionalized Fe_3O_4 NPs at different Fe concentrations for 4 h.

Fig. 6. *In vivo* MR images (a) and MR signal intensity (b) of tumors after intravenous injection of the FA-functionalized Fe_3O_4 NPs ([Fe] = 80 mM, 0.1 mL PBS) to tumor-bearing mice at different time points (Group 1). For comparison, mice were also intravenously (Group 2) or intratumorally (Group 3) injected with free FA (20 mM, 0.1 mL PBS) for 30 min to block the FAR expression before the administration of the FA-functionalized Fe_3O_4 NPs.

Fig. 7. Blood smears and H&E stained tissue sections from mice at 10 days post intravenous injection of the FA-functionalized Fe_3O_4 NPs ([Fe] = 80 mM, 0.1 mL PBS) and mice without treatment. The scale bar in each panel represents 50 μm.

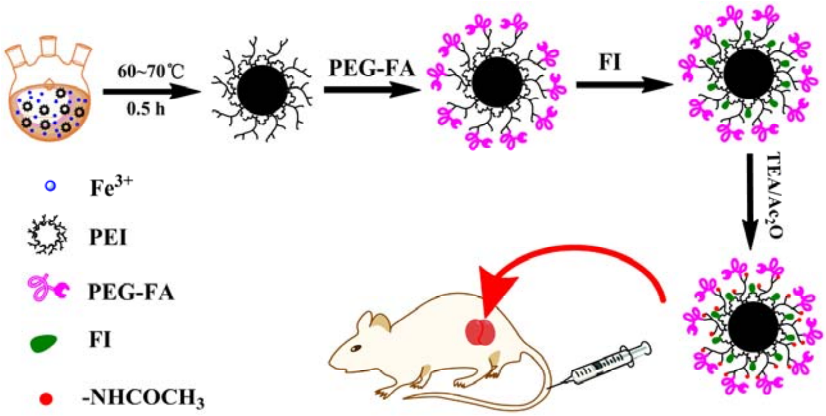

Scheme 1

Li *et al*.

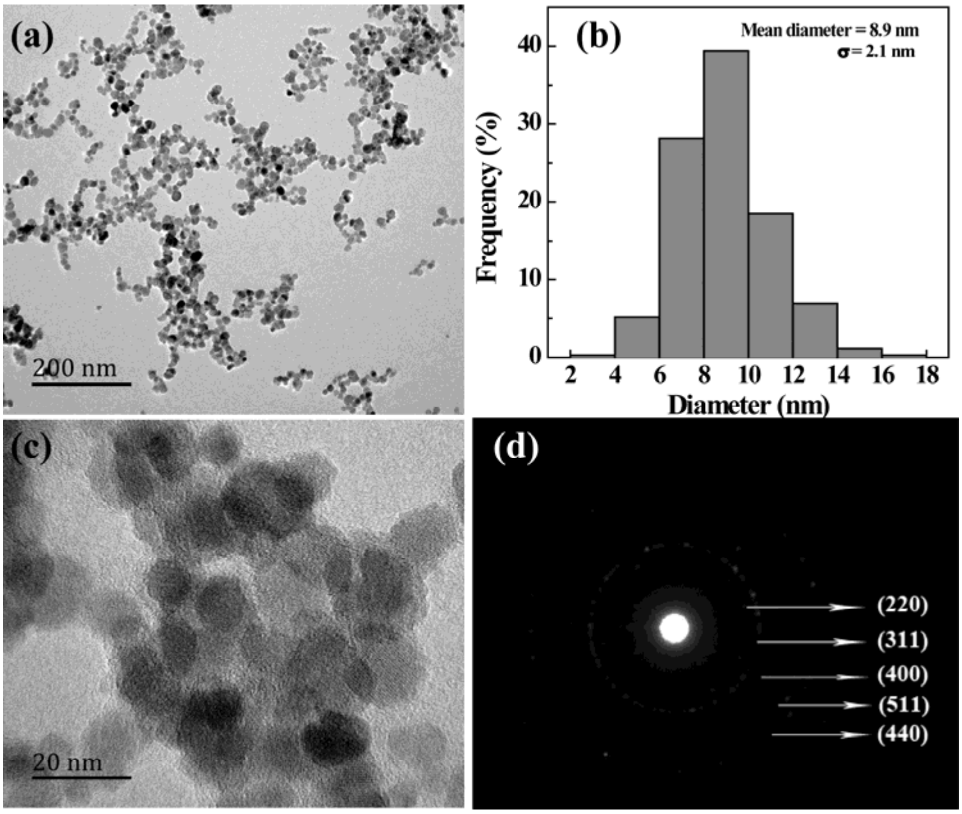
(a)
200 nm
(b)
Mean diameter = 8.9 nm
σ = 2.1 nm
Frequency (%)
0
10
20
30
40
2
4
6
8
10
12
14
16
18
Diameter (nm)
(c)
20 nm
(d)
(220)
(311)
(400)
(511)
(440)

Fig. 1

Li *et al.*

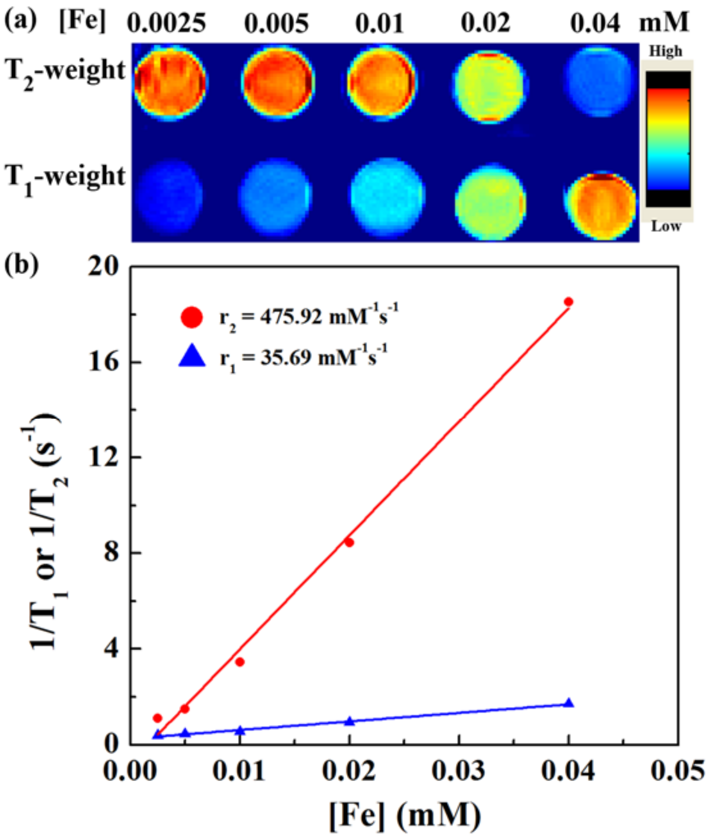
(a) [Fe] 0.0025 0.005 0.01 0.02 0.04 mM
T2-weight
T1-weight
High
Low
(b)
r2 = 475.92 mM-1s-1
r1 = 35.69 mM-1s-1
1/T1 or 1/T2 (s-1)
[Fe] (mM)
0 4 8 12 16 20
0.00 0.01 0.02 0.03 0.04 0.05

Fig. 2

Li *et al.*

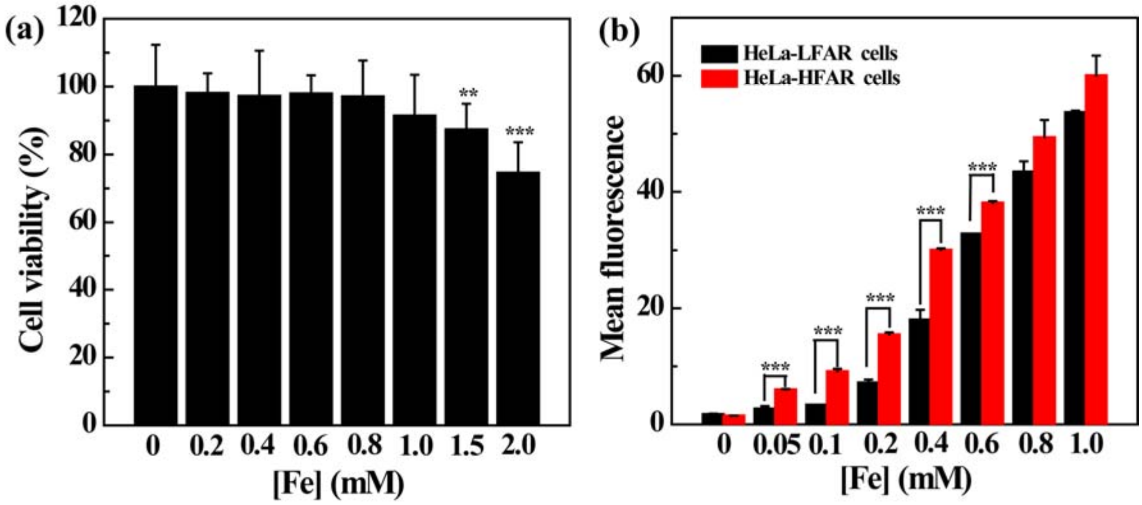
(a)
Cell viability (%)
120
100
80
60
40
20
0
**
***
0
0.2
0.4
0.6
0.8
1.0
1.5
2.0
[Fe] (mM)
(b)
HeLa-LFAR cells
HeLa-HFAR cells
Mean fluorescence
60
40
20
0
***
0
0.05
0.1
0.2
0.4
0.6
0.8
1.0
[Fe] (mM)

Fig. 3

Li *et al*.

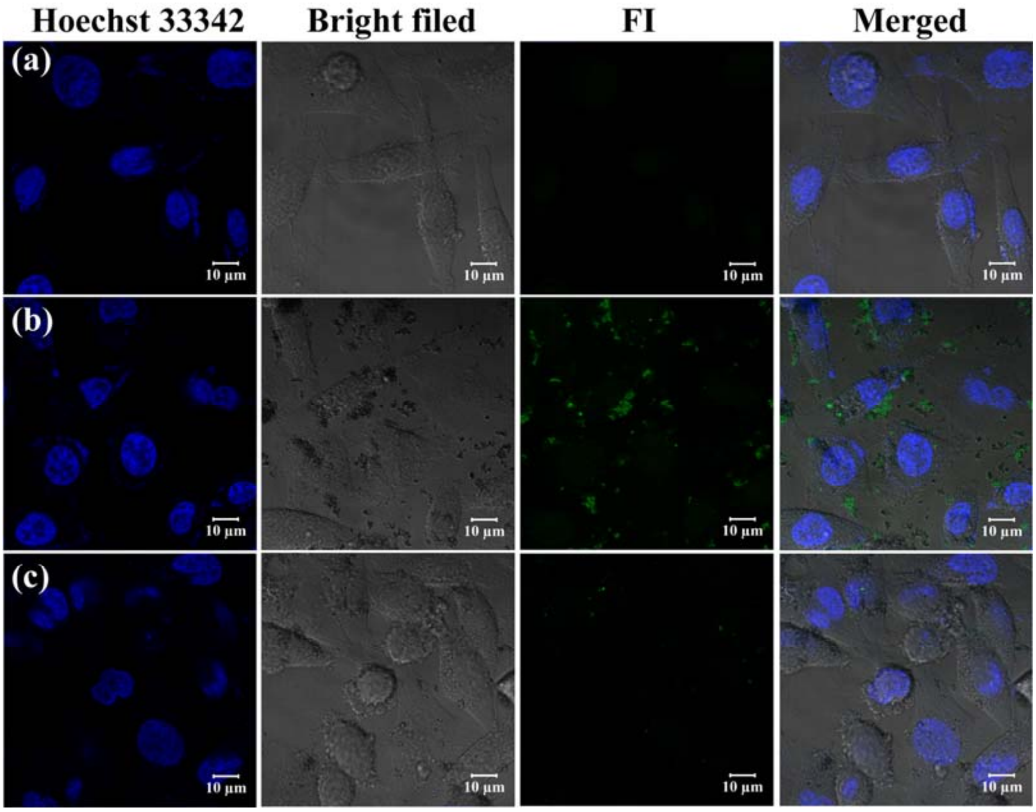

Fig. 4

Li *et al.*

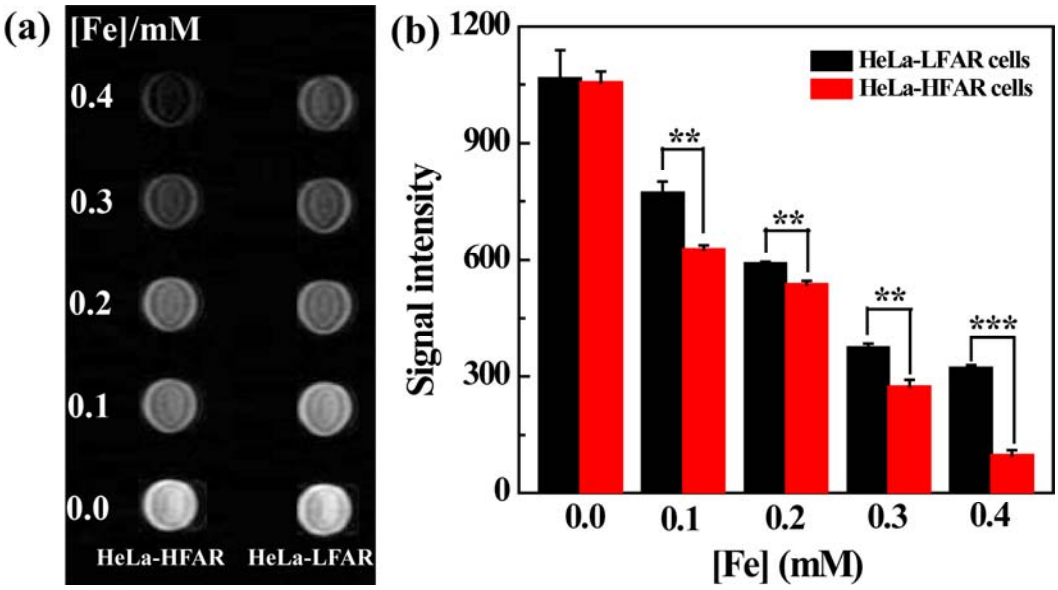
(a)
[Fe]/mM
0.4
0.3
0.2
0.1
0.0
HeLa-HFAR
HeLa-LFAR
(b)
HeLa-LFAR cells
HeLa-HFAR cells
Signal intensity
1200
900
600
300
0
**
**
**
***
0.0
0.1
0.2
0.3
0.4
[Fe] (mM)

Fig. 5

Li *et al.*

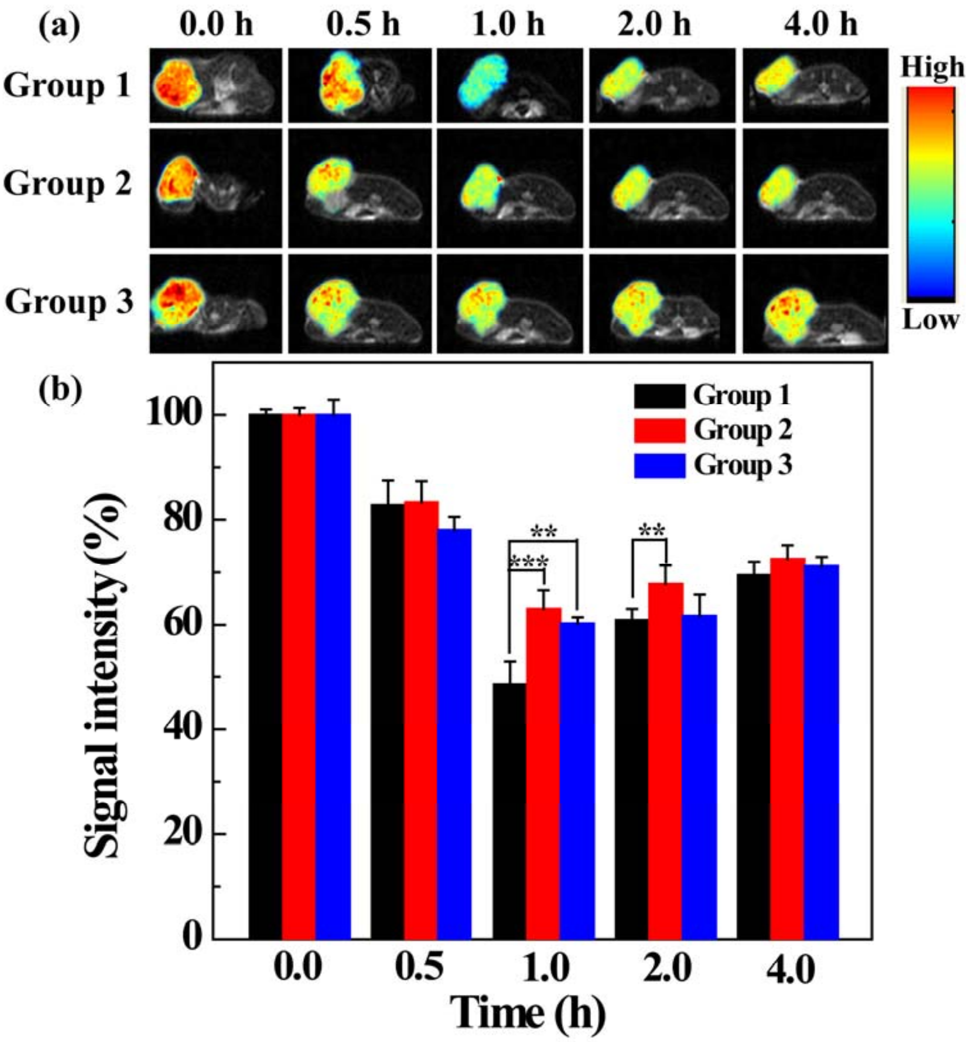

(a)
0.0 h
0.5 h
1.0 h
2.0 h
4.0 h
Group 1
Group 2
Group 3
High
Low
(b)
Signal intensity (%)
Time (h)
Group 1
Group 2
Group 3
**
***
**

Fig. 6

Li *et al.*

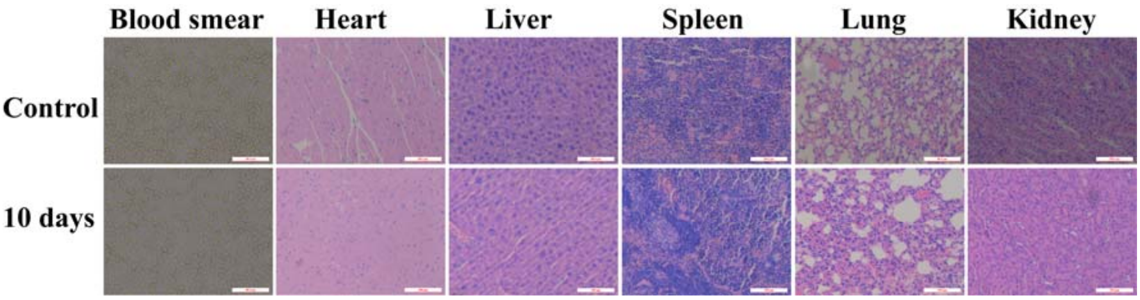

Fig. 7

Li *et al.*

Table of Contents (TOC)

Facile synthesis of folic acid-functionalized iron oxide nanoparticles with ultrahigh relaxivity for targeted tumor MR imaging†

Jingchao Li,[a1] Yong Hu,[a1] Jia Yang,[b1] Wenjie Sun,[a] Hongdong Cai,[c] Ping Wei,[a] Yaping Sun,[d]* Guixiang Zhang,[b] Xiangyang Shi,[a, c]* Mingwu Shen[a]*

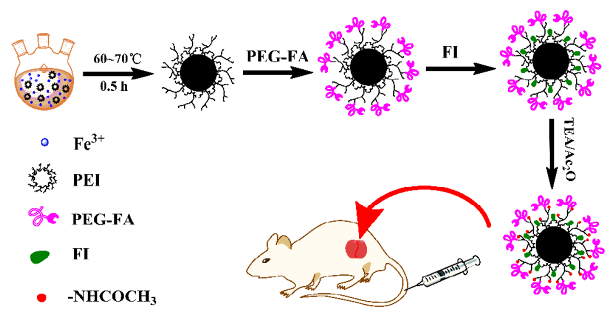

Folic acid-functionalized iron oxide nanoparticles with an ultrahigh r_2 relaxivity can be formed for targeted MR imaging of tumors.